Light Metals 2015
Edited by: Margaret Hyland
TMS (The Minerals, Metals & Materials Society), 2015

Light Metals 2015

CAST SHOP FOR ALUMINUM PRODUCTION

General Cast Shop

SESSION CHAIR
Mohamed Ali
Masdar Institute
Abu Dhabi, United Arab Emirates

Light Metals 2015
Edited by: Margaret Hyland
TMS (The Minerals, Metals & Materials Society), 2015

Deformation of the Aluminum Bath Surface in an Induction Melting Furnace

Akshay Bansal[1], Pierre Chapelle[1], Yves Delannoy[2], Emmanuel Waz[3], Pierre Le Brun[3], Jean Pierre Bellot[1]

[1] Institut Jean Lamour, UMR 7198, Université de Lorraine, CNRS - LabEx DAMAS, CS 50840, Parc de Saurupt, 54011 Nancy, France
[2] SIMaP, Grenoble-INP, UJF, CNRS, BP 75, 38402 St. Martin d'Hères, France
[3] Constellium Technology Center, CS 10027, 38341 Voreppe Cedex, France

Keywords: Induction Melting, Aluminum Bath, Free Surface Deformation, Measurement, Simulation

Abstract

The electromagnetic forces in an induction furnace deform the free surface of a molten aluminum bath into a dome shape. The deformation may also be affected by the oxide skin present at the free surface. A structured light technique was used to measure the free surface deformation and its variations in a laboratory scale induction furnace, as a function of operating parameters – current intensity and liquid metal filling inside the crucible. A numerical model capable of taking into account the strong electromagnetic – hydrodynamics coupling was developed to simulate the electromagnetic stirring phenomena. The Volume Of Fluid (VOF) method was applied to model the free surface deformation. A comparison of the measured and the calculated dome shapes is presented.

Introduction

The processing of aluminum alloys in an induction melting furnace is an established industrial practice. The induction furnace which is based on the principles of electromagnetics, allows non–intrusive stirring and heating of the metal bath [1]. The free surface of the metal bath in the induction furnace deforms and takes the shape of a dome. The dome shape is due to a delicate equilibrium between the electromagnetic forces, the hydrodynamic pressure, the gravitational force and the surface tension force.

In the case of an aluminum alloy, since the induction process often takes place under atmospheric conditions, the free surface is instantaneously covered by an oxide skin. The impact of this oxide skin on the deformation of the free surface and on the hydrodynamics of the metal bath is a point that has received little attention in the literature and is one of the main topics addressed in the present work.

Only a few references are available in the literature concerning experimental measurement of the free surface deformation of a metal bath during induction melting. Etay et al. [2] and Fautrelle et al. [3] studied mercury and gallium baths respectively using a contact probe. The probe was well adapted to a temperature range of 20 – 70 °C, with a precision of ±0.5 mm. Kirpo [4] also used a contact probe to measure the free surface deformation of a Wood's metal bath ($T_m \approx 70$ °C). The contact probe technique is difficult to adapt for aluminum baths as the temperature range is more than 700 °C. Moreover, these experiments only provide non instantaneous discrete measurements (up to 20 points) of the free surface which are inadequate for a complete free surface description.

The stirring of the liquid metal in an induction furnace is often turbulent in nature. A proper modeling technique is required to model such turbulent flows. El Keddah et al. [5] and Umbrashko et al. [6] used RANS modeling, using a two equation model such as k-ε or k-ω. Scepanskis et al. [7] and Spitans et al. [8] have recently used the k-ω SST model. A common feature among these numerical models was a one-way coupling between the electromagnetics and the hydrodynamics. The Lorentz forces in the bath were calculated separately and subsequently coupled with the fluid flow. Delannoy et al. [9] proposed a stronger coupling whereby the Lorentz forces were calculated at the same time as the hydrodynamics. In this manner the Lorentz forces were calculated while taking into account an updated free surface deformation at each time step. Modeling of the free surface deformation is also discussed by Courtessole and Etay [10] in their recent work.

The oxidation of the free surface on an aluminium bath may have different impacts on the hydrodynamics of the bath. The main impact studied in the literature concerns the influence of the oxide skin on the surface tension of the metal. Several techniques such as the sessile drop method or the maximum bubble pressure method (for example by Goumiri et al. [11]) were used to measure the surface tension of a liquid aluminum bath sample. It was found that the surface tension for 99.99 % pure aluminum decreases from 1.1 N/m to 0.86 N/m as the surface oxidation increases, as presented by Garcia-Cordovilla et al. [12].

This paper deals with the description, both experimental and numerical, of the free surface deformation of an aluminum bath during induction melting. In the following sections, the experimental method based on a structured light projection technique is described. Then, we focus on the numerical model developed to simulate the various physical phenomena involved in an induction furnace. Experimental and numerical results obtained for a laboratory scale induction furnace are thereafter presented and compared.

Experimental Method

Description of the installation

A schematic of the induction furnace installed at Jean Lamour Institute is presented in Figure 1. The inductor consists of an 8 turn coil. The interior diameters of the alumina crucible and the inductor are 106 mm and 200 mm respectively. Their corresponding heights are 200 mm and 250 mm respectively. The crucible rim is offset by 5 mm with respect to the inductor's top.

The maximum liquid metal filling inside the crucible corresponds to 4 kg of aluminum alloy: Al-1xxx (with at least 99% aluminum).

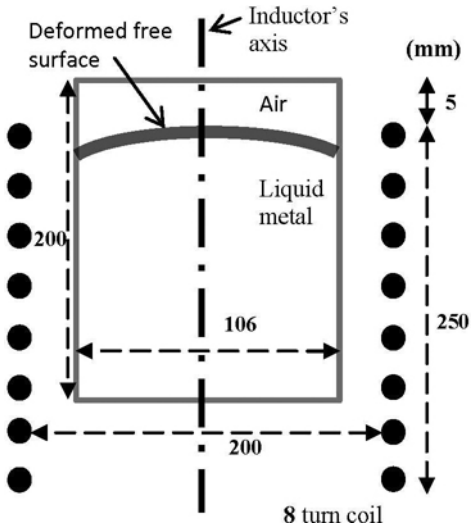

Figure1: Induction furnace schematics

Description of experimental technique – Structured Light

The structured light technique was used to measure the temporal evolution of the complete free surface deformation. The technique is widely used in medical imaging, automobile modeling, profiling and architecture. No particular application in the liquid metal domain was found in the literature. Geng [13] can be consulted for a review of the structured light techniques. This technique which allows rapid real time acquisition of a complete surface basically consists of projecting a band pattern onto the surface under study. Any surface deformation will consequently deform the projected pattern which is captured as an image by a camera. The processing of the captured images using the principle of triangulation enables the 3D profile of the surface to be determined as shown in Figure 2.

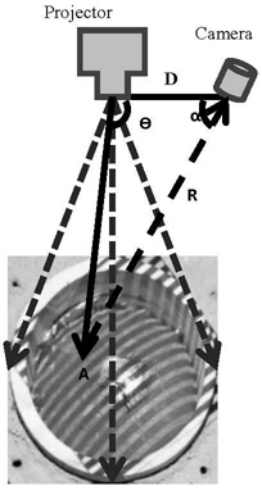

Figure 2: Structured light technique – pattern projection

As shown in Figure 3, the complete optical system was mounted on an optical bench support which maintained the calibration of the system. The support also provided a degree of freedom along the z-axis for unidirectional translation of the complete setup. The optical system was calibrated to be approximately 800 mm away from the observed surface which was considered as the reference plane. Almost 100 mm of deformation along the z-axis, with respect to the reference plane could be measured using the system (Figure 3). A company specialized in optical metrology – Holo3 [14] participated in the experimental campaign by supplying the optical system along with the post processing software.

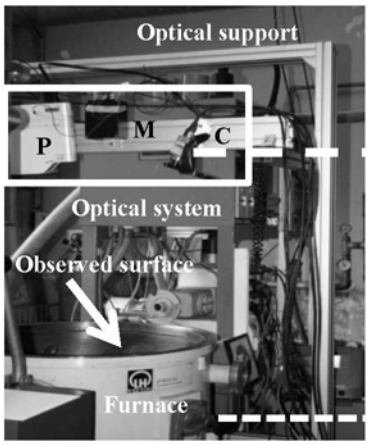

Figure 3: IJL – Induction furnace with mounted optical system (P: Projector, M: Modulator, C: Camera)

Each pixel on the structured light pattern has an intensity I_{xy} associated with it, where x and y represent the coordinates of the projected pattern. The key aspect of recreating the complete surface lies in distinguishing each pixel, which is performed by using the sequential or the single shot method.

Sequential hybrid method

The sequential hybrid method of phase shift with black and white pattern involves projecting a sequence of carefully designed variable fringe patterns. This is a two-step method. The first step consists of considering a black and white binary pattern (Figure 4a) with a given step size as a base image. During the second step, several sinusoidal fringe patterns with a phase shift are projected onto the surface. The two steps are then repeated for the next pattern step size. The ensuing calculation of the phase shift enables the calculation of the surface deformation using the principle of triangulation. This technique provides an accurate evaluation of the spatial deformation of the free surface but averages out any high frequency fluctuations while performing the step variation along with the phase shifting. The hybrid sequential technique enables measurements with a precision of ±0.1 mm at a frequency of 0.03 Hz. This was repeated for 180 s to describe the temporal evolution of the free surface. In order to remove any shadowed zones, two cameras were used, and their images were combined to give a complete measurement of the observed surface.

Single shot method

This method is based on the projection of a single pattern. It was used to study the temporal evolution at a higher frequency of 1 Hz and is therefore suitable for dynamic surfaces but with a reduced measurement precision of ±1 mm. The projected black and white stripe pattern is distorted according to the observed surface geometry (Figure 4b). The image of the deformed pattern captured by the camera is then processed by analyzing (Fast Fourier

Transformation) the variation of the step size (d1, d2) between stripes. Once the phase for each pixel is found, the principle of triangulation calculates the displacement of the 3D surface.

Figure 4a: Step variation for sequential hybrid method

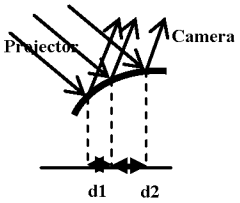

Figure 4b: Single shot technique – deformed pattern captured by a camera

Operating parameters

During the experimental campaign, measurements were performed while varying the operating parameters. In this paper, we have focused only on one operating parameter set: a metal filling of 75 % (for a maximum of 4 kg of Al-1xxx) and a generator power of 15 kW. The corresponding initial filling level was measured and equal to 157 mm. Simultaneously a Rogowski coil measured the current intensity as 1507 A (±1 %) while the current frequency was noted as 3500 Hz.

Numerical Model

Although the induction furnace coil has a helix design, a hypothesis of perfect axisymmetric geometry of the coil has been taken in order to simplify our model and lighten the calculation load. Moreover, the experimental results show that the free surface is almost symmetric with respect to the axis of the coil (discussed in the next section). This justifies our 2D axisymmetric approach to the modeling of the induction furnace. The cylindrical coordinate system (r,θ,z) is thus best suited to express the various governing equations of the phenomena considered in our numerical model, which are as follows:

- The electromagnetics of an inductor
- The turbulent flow of the liquid metal inside the crucible
- The deformation of the free surface of the metal bath
- The presence of an oxide skin covering the metal bath

It was considered that the temperature in the stirred metal bath was homogeneous and thus the energy equation was not solved. The model uses ANSYS Fluent platform to calculate the hydrodynamics of the liquid metal bath while separate User Defined Functions (UDF) are used to calculate the induction equation and the oxide skin effects.

The electromagnetics of an inductor

The induction phenomena are modeled by a set of UDFs – Induc 14.0.0.1, provided by SIMAP laboratory in Grenoble. This set of UDFs solves the induction equation under the *quasi-steady* hypothesis of electromagnetism by using the potential vector (**A**) – scalar electric potential (V) formulation. This modeling approach is found in Lacombe et al. [15] and Courtessole and Etay's study [10] among others. The potential vector **A** is a solution of the induction equation presented here in its complex partial differential form:

$$\Delta \mathbf{A}_\theta - i\mu_0\sigma\omega\mathbf{A}_\theta e^{i\omega t} + \mu_0 j = 0 \qquad (1)$$

Where $\boldsymbol{A_\theta = A_\theta}^r + i\boldsymbol{A_\theta}^i$. ω, σ and μ_0 are respectively the electrical current pulsation, the electric conductivity and the magnetic permeability constant. It is then possible to calculate the distributions in the liquid metal bath of the magnetic field density **B**, the induced current density $\boldsymbol{j}$ and the Lorentz force **F** (Table 1).

Table 1: Variables calculated from the solution of A

Magnetic field	$\mathbf{B} = \nabla \times \mathbf{A}$
Current density	$\boldsymbol{j} = (\nabla \times \mathbf{B})/\mu_0$
Lorentz force	$\mathbf{F} = \mathbf{j} \times \mathbf{B}$

Turbulent flow of the metal

The continuity equation and the Navier-Stokes equation govern the liquid flow inside the metal bath.

$$\frac{\partial \rho}{\partial t} + \frac{\partial (\rho u_j)}{\partial x_j} = 0 \qquad (2)$$

$$\frac{\partial (\rho u_i)}{\partial t} + \frac{\partial (\rho u_i u_j)}{\partial x_j} = -\frac{\partial p}{\partial x_i} + \frac{\partial}{\partial x_i}\left(\mu_{ef}\frac{\partial u_i}{\partial x_j}\right) + \rho g_i + f_{Lorentz,i} \qquad (3)$$

u, ρ, μ_{ef} and p are respectively the velocity vector, the density, the dynamic effective viscosity, the pressure and the external forces. The last term in Eqn. 3 represents the Lorentz force.

Such a stirred flow is turbulent in nature. Instead of using the k-ε or the k-ε RNG method as carried out by Baake et al. [16] and Courtessole and Etay [10], we have selected a variant of the k- ω model. The k-ω Shear Stress Transport (SST) model, proposed by Menter [17] brings together the best features of the k-ω and k-ε turbulence models: k-ω is used in the inner regions of the boundary layers near the walls and k-ε is used in regions away from the wall. This model involves solution of two transport equations for the turbulent kinetic energy (k) and its specific dissipation rate (ω).

When treating free surface flows, turbulence damping in the interfacial region is required to conserve the accuracy of the model. This is ensured by adding a damping term in the ω equation (option available in ANSYS Fluent).

Free surface deformation

It is obvious that a correct computation of hydrodynamics in metal bath requires an accurate representation of its free surface. The method selected in the present work is the Volume Of Fluid (VOF) method proposed by Hirt and Nichols [18], where a scalar indicator binary function (α) is used to distinguish between the metal and air regions. The volume fraction of metal within a control volume is used to define the indicator function. The interface is present in a control volume if the following expression is satisfied: $0 < \alpha < 1$. The evolution of the volume fraction inside a control volume is calculated by solving the transport equation:

$$\frac{\partial \alpha}{\partial t} + u_i \frac{\partial \alpha}{\partial x_i} = 0 \qquad (4)$$

Oxide skin effects

The oxide skin which covers the free surface of the metal bath is considered homogeneous, though some stretched regions were observed during some of the experiments. The oxide skin is

treated as a pseudo deforming wall, which impacts the hydrodynamics of the metal bath in two different ways.

At the free surface, the oxide skin modifies the surface tension of the free surface. The effective surface tension force occurring at the bath free surface is modeled by adding an equivalent volumetric source term in the Navier-Stokes equations in the interfacial cells using existing functionalities of the ANSYS Fluent software. The curvature in each interface cell is calculated as: $\kappa = \nabla \cdot \vec{n}$, where the interface normal vector is calculated from the volume fraction of the metal: $\vec{n} = \nabla\alpha / \|\alpha\|$.

In the tangential direction to the interface, it is considered that the oxide skin behaves like a pseudo wall and thus exerts a friction force on the metal free surface. The friction force is described as a surface force in Eqn. 5:

$$\overrightarrow{\tau_{oxide}} = -C_f\left(\overrightarrow{V_{m,i}}.\vec{t} - \overrightarrow{V_{oxide}}\right)\vec{t} = -C_f\left(\overrightarrow{V_{m,i}}.\vec{t}\right)\vec{t} \qquad (5)$$

In our model, the surface force is translated into a volumetric force source term as described in Eqn. 6, which is taken into account in the N-S equations:

$$\overrightarrow{F_{vol}} = \overrightarrow{\tau_{oxide}}\, A_i = -C_f A_i\left(\overrightarrow{V_{m,i}} \cdot \vec{t}\right)\vec{t} \qquad (6)$$

C_f, $V_{m,i}$ and A_i respectively are an adjustable friction coefficient, the metal velocity near the interface and the interfacial area density in the interfacial cell. During the implementation phase, it was demonstrated that high values of C_f (above 1500 $kg.m^{-2}.s^{-1}$) are required for the oxide skin to be assimilated to a wall. For suitably high values of C_f, the flow solution is not sensitive to the precise value of C_f. The velocity at the interface tends towards zero, leading to the formation of a boundary layer on the interface.

Numerical model – initial and boundary conditions

At each time step of the calculation, the Lorentz force distribution is supplied to the metal bath calculation. The updated free surface deformation is then provided back to Induc 14.0.0.1 to continue the next time step of the strongly coupled modeling.

The previously described model was employed to simulate the experiment reported above. ANSYS Workbench tools – *Design Modeler* and *Meshing* were used to create the geometry (Figure 5a) and the mesh (Figure 5b).

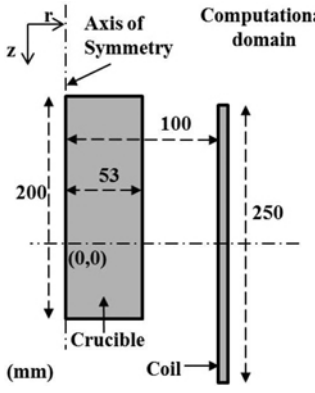

Figure 5a: Geometry

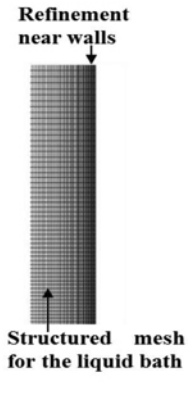

Figure 5b: Zoomed up crucible mesh

The inductor has been represented as one single continuous sheet instead of eight individual coils. Although in reality the crucible has a round bottom, to simplify a rectangular bottom geometry was created.

The crucible volume and coil were meshed in a structured manner with a refinement at the crucible walls. The number of mesh cells equals to 21200 in the crucible region, 250 in the coil and 7382 in the gas region. The mesh maximum skewness in the gas region lies around 0.75 which is satisfactory. The smallest cell size in the crucible region is 275 µm × 125 µm. An overall computational domain ten times the size of the coil encloses the crucible and the coil. Some thermophysical properties of the aluminum alloy series 1xxx are summarized in Table 2.

Table 2: Al-1xxx properties

Density ($kg.m^{-3}$)	Dynamic Viscosity (Pa.s)	Surface tension ($N.m^{-1}$)	Electrical conductivity $(ohm.m)^{-1}$
2379	1.15×10^{-3}	0.865	3.97×10^{6}

A constant specified zero value of vector potential A_θ on exterior walls of the computational domain was imposed as a boundary condition. Also a Neumann boundary condition on the axis of the crucible was imposed: $\left.\frac{\partial A_\theta}{\partial r}\right|_{r=0} = 0$. At the crucible walls, a no slip condition was used resulting in a zero liquid metal velocity. Model input parameters correspond to the operating parameters previously discussed. An initial value of zero turbulent kinetic energy and a very small initial dissipation rate equal to 0.002 s^{-1} were applied. A fixed time stepping method was selected with a time step of 0.5 ms. The transient simulation was performed until a steady state of the flow was established.

Results and Discussion

Experimental results

Figure 6 illustrates a processed image of the free surface showing a two dimensional contour of the relative height for each pixel of the surface.

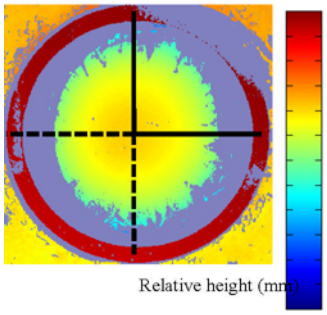

Figure 6: Processed image of the deformed surface

The outer band (in red color) represents the crucible rim while the central disc represents the deformed free surface. No information for the near wall area is available since the reflected fringe patterns were shadowed by the crucible wall. Nevertheless, over the complete free surface, more than 60% of the surface has been measured. A comparison of four vertical cross-sections of the free surface profile has confirmed an almost symmetric nature of the free surface dome. The averaging of these sections allows an average dome profile to be obtained, which is presented in Figure

7. To add to it, the relative position of the crucible rim and the near wall zone (no measurement due to shadows) can also be observed in Figure 7.

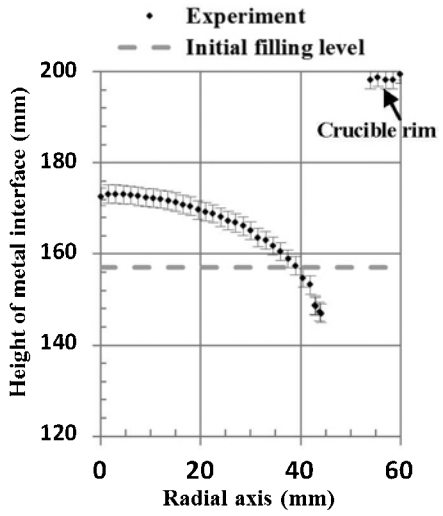

Figure 7: Average dome profile along with its deviation

The investigation of the temporal evolution of the free surface deformation provided limited conclusions. The fluctuations were within the precision range for the single shot technique while for the hybrid sequential technique, the total sample size of 6-8 measurements was insufficient to draw any statistical correlation. Additionally the hybrid sequential technique measured the dome profile deviation as ±2 mm during the series of measurements. Thus an average dome profile along with its range of deviation was obtained as presented in Figure 7.

Numerical model results and Comparison

Figure 8a shows the flow structures inside the liquid metal bath and the distributions of the metal velocity. The steady state flow has three recirculation zones: one within the dome, another in the central region and a third and the fastest in the bottom corner of the crucible. The average velocity in the bath is 0.16 m/s.

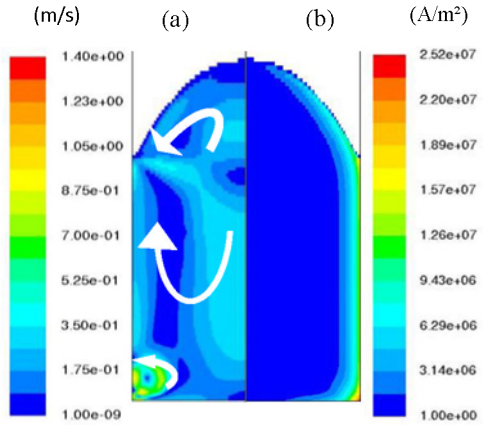

Figure 8 a) Liquid metal velocity distribution (m/s)
b) Induced current density distribution (A/m²)

Figure 8b presents the distribution of the induced current density in the metal bath. With a maximum of 2.52×10^7 A/m² inside the metal bath, it is observed that the current density is concentrated near the crucible wall, which follows the theoretical concept of the electromagnetic skin effect. The current density decreases rapidly to low values within 10 mm from the wall. An order of magnitude of the skin depth is found equal to $\delta = 4.5$ mm, which is comparable to the skin depth calculated theoretically $\delta = (\pi\mu\sigma f)^{-0.5} = 4.27$ mm. The orders of magnitude of the Lorentz force and the melt velocity are in the same range as that seen in modeling results for similar sized induction furnaces in the papers [4], [7] and [8].

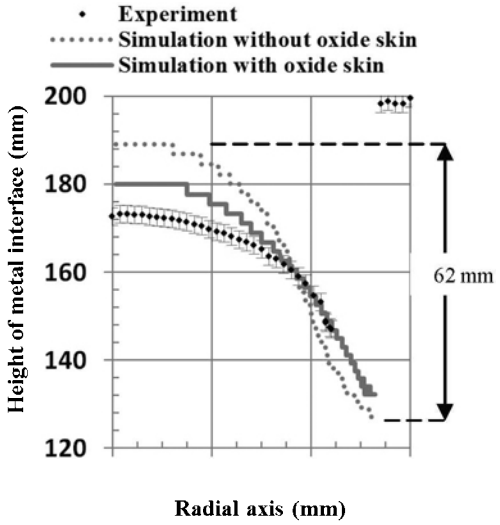

Figure 9: Comparison between the measured and calculated free surface dome profiles

Figure 9 presents the calculated free surface dome profile with and without the oxide skin. Without the oxide skin, the maximum height of the interface at the axis is 190 mm while the dome height is 62 mm. The dome undergoes a significant change with the addition of the friction force due to the oxide skin and reduces by almost 10 mm along the axis. These profiles are compared with the measured dome profile. The profile with the friction force is much closer to the measured profile. Nevertheless a difference between the two profiles is noticeable, especially at the axis of symmetry. The difference was examined through testing of the following hypotheses:

- Could the temperature governed variation of the metal bath viscosity change the dome profile?

The simulation presented in the above section was performed using the dynamic viscosity value in Table 2, which corresponds to the value at 700 °C. During the experimental campaign, it was observed that for the given set of operating parameters, heat accumulated in the metal bath over the course of time. The temperature of the metal bath thus evolved from the melting point to a measured temperature equal to almost 1000 °C. Therefore we wanted to study the impact of the temperature evolution on the dome profile. According to Roach and Henein [19], a rise in the temperature from 700 °C to 1000 °C results in a viscosity drop of almost 40 %, from 1.15 mPa.s to 0.71×10^{-3} mPa.s. Thus in order to study the effect of the temperature dependence of the viscosity, an additional simulation with a modified viscosity value (0.71×10^{-3} mPa.s) was carried out. The outcome confirmed that though the flow structures of the metal bath were modified, the dome profiles remained identical.

- Does the turbulence damping model near the metal bath free surface impact the dome profile?

The turbulence damping term includes an adjustable factor. Simulations were launched to test the sensitivity of the dome profile with respect to the adjustable factor variation. Results confirmed that the dome profiles remain unchanged as a function of the adjustable factor.

- How important is the representation of the inductor setup in the numerical model?

The difference between the real inductor setup (disjointed 8 turn coil - Figure 1) and its corresponding representation in the numerical model (a continuous sheet – Figure 5a) may lead to a difference in the real and the calculated magnetic field generated by the inductor. This in turn may impact the free surface deformation of the metal bath. Centerline profile of the axial magnetic field was measured inside an empty crucible (without any metal) and found to be lower than the calculated magnetic field. This could possibly explain the difference in the measured and the calculated dome profile.

Conclusions & Future work

A non-intrusive structured light technique was used to measure the free surface deformation of an aluminum bath in a laboratory scale induction furnace. The results obtained in the form of an averaged 3D dome profile confirm the axisymmetric nature of the dome while also providing a far more complete picture of the entire free surface compared to earlier techniques.

The hydrodynamics of the metal bath represented by a 2D axisymmetric geometry and the deformation of its free surface were simulated using the platform provided by ANSYS Fluent while UDF's were plugged in to calculate the electromagnetics and to account for the effect of the oxide skin covering the free surface. A marked impact on the dome profile was observed, when taking the oxide skin friction force into account. The oxide skin noticeably reduces the calculated maximum height of the interface at the axis by almost 10 mm for the reference case. Although the model overestimates the dome height when compared to the measured deformation, the numerical results in general (dome shape and order of magnitude) are satisfactory. It was noted that the simplified representation of the inductor setup in the model could possibly be the reason behind the overestimation. Modeling of other induction furnaces with different design and operating parameters is feasible using this numerical tool. It should provide a reasonable description of the induction furnace phenomena, especially the free surface deformation of the metal bath. Of course the quality of the results will be subject to the quality of the numerical model input parameters.

Acknowledgements

This research has been supported by the French National Research Agency within the framework of an ANR project PRINCIPIA, *Procédés industriels de coulée innovants pour l'industrie aéronautique* (2010-RMNP-0007).

References

1. Davidson, P. A, An Introduction to Magnetohydrodynamics (2001) Cambridge University Press.
2. Etay, J., Dumont, B., Hamburger, J., Bolcato, R., Haettel, R., "Resistive probe for continuous measurement of electroconductive liquid levels facing electromagnetic fields." Exp in Fluids **32**(4) (2002), 518-526.
3. Fautrelle, Y., Perrier, D., Etay, J., "Free surface controlled by magnetic fields." ISIJ International **43**(6) (2003), 801-806.
4. Kirpo M. "Modeling of Turbulence Properties and Particle Transport in Recirculated Flows." (2008) (PhD thesis, U Latvia).
5. El-Kaddah, N., Szekely, J., Taberlet, E., Fautrelle Y., "Turbulent recirculating flow in induction furnaces: A comparison of measurements with predictions over a range of operating conditions." Metall Mater Trans B **17**(4) (1986), 687-693.
6. Umbrashko, A., Baake, E., Nacke, B., Jakovics A., "Modeling of the turbulent flow in induction furnaces." Metall Mater Trans B **37**(5) (2006), 831-838.
7. Scepanskis M., Jakovics, A., Baake, E., Nacke, B., "Solid inclusions in an electromagnetically induced recirculated turbulent flow: simulation and experiment". Int J Multiph Flow. **64** (2014), 19-27.
8. Spitans S, Jakovics, A., Baake, E., Nacke, B., "Numerical Modeling of Free Surface Dynamics of Melt in an Alternate Electromagnetic Field: Part I. Implementation and Verification of Model". Metall Mater Trans B. **44**(3) (2013), 593–605.
9. Delannoy, Y., Garnier, C., "Free Surface Shape in Induction Furnaces: Influences of the Stirring motion on the mean dome height". (2006) (Proceeding at 5th Int. Conf. Electromagnetic Processing of Materials, Sendai, Japan).
10. Courtessole, C., Etay, J., "Flows and mass transfers in two superimposed liquid layers in an induction furnace". Int J Heat Mass Tran **65**(2013), 893–906.
11. Goumiri, L., Joud, J.C., Desre, P., "Tensions superficielles d'alliages liquides binaires présentant un caractère d'immiscibilité: Al-Pb, Al-Bi, Al-Sn et Zn-Bi." Surface Science **83**(2) (1979), 471-486.
12. Garcia-Cordovilla, C., Louis, E., Pamies, A., "The surface tension of liquid pure aluminium and aluminium-magnesium alloy." J of Mat Sci **21**(8) (1986): 2787-2792.
13. Geng, J. "Structured light 3D imaging – a tutorial". Advances in Optics and Photonics, **3**(2)(2011), 128-160.
14. Holo3 – A structured light tutorial, "Les techniques de lumière structurée –la mesure de forme et de déformations par projection de franges", Saint Louis, France. www.holo3.com.
15. Lacombe, J.G., Delannoy, Y., Trassy, C., "The role of radiation in modelling of argon inductively coupled plasmas at atmospheric pressure." J. of Phy D: App. Phy **41**(16)(2008),165204.
16. Baake, E., Nacke, B., Umbrashko, A., Jakovics, A., "Turbulent flow dynamics, heat transfer and mass exchange in the melt of induction furnaces", COMPEL - Intl J Computation and Mathematics in Electrical and Electronic Eng. **22**(1)(2003), 39-47
17. Menter F.R., "Two-equation eddy-viscosity turbulence models for engineering applications", AIAA-Journal, **32**(8)(1994).
18. Hirt, C.W., Nichols, B.D., "Volume Of Fluid (Vof) Method For The Dynamics Of Free Boundaries". J Of Comp Phy, **39**(1)(1981), 201-225.
19. Roach, S.J., Henein, H., "A New Method to Dynamically Measure the Surface Tension, Viscosity, and Density of Melts". Metall Mater Trans B. **36**(10) (2005), 667-675.